Physically Based Model for Evaluation of Rock Scour due to High-Velocity Jet Impact

Erik F. R. Bollaert, M.ASCE,[1] and Anton J. Schleiss[2]

Abstract: Scour of rock may occur downstream of dam spillways, as a result of the impact of high-velocity jets. The phenomenon is traditionally assessed by means of (semi-) empirical methods. These partially neglect basic physical processes responsible for rock mass breakup. Therefore, a model to evaluate the ultimate depth and time evolution of scour in jointed rock is presented. The model is based on near-prototype scaled experimental investigations of transient water pressures in artificially created rock joints and on a numerical modeling of the measured pressures. It describes two different ways of rock mass destruction, i.e., failure by instantaneous or progressive breakup of closed-end rock joints, and failure by dynamic ejection of single rock blocks. The corresponding computational methods are easily applicable to practice, without neglecting relevant physics. The basic principles are outlined and applied to the well-known scour hole at Cabora-Bassa Dam.

DOI: XXXX

CE Database subject headings: Rocks; Scour; Spillways; Fractures; Uplift; Dam safety.

Introduction

Rock scour due to high-velocity jet impact downstream of dams and hydraulic structures has mostly been studied by empirical or semiempirical approaches. These approaches are hardly applicable outside the range of parameters for which they have been defined and partially neglect fundamental physical principles that characterize scour (Schleiss 2002; Bollaert and Schleiss 2003a). Moreover, most of them have been developed based on scaled model experiments and exhibit significant scaling effects when applied to prototype cases. A detailed state-of-the-art review of rock scour due to jet impact can be found in Bollaert and Schleiss (2003a).

A major problem during model tests is to simulate the breakup phase of the rock mass, i.e., the stage of formation and propagation of rock joints until the rock mass is transformed into an ensemble of distinct blocks. Several investigators have tried to bypass this aspect by using binders, such as clay, paraffin, etc., in their experiments (Johnson 1977; Quintela and Da Cruz 1982). These provide a retardation of the scour formation and more realistic scour geometries, but cannot provide a plausible substitute for the complex behavior of partially jointed rock.

Dynamic pressures at plunge pool bottoms and in stilling basins have first been studied in the 1960s. Transfer of these pressures to joints between the slabs or blocks was found to result in catastrophic failure by dynamic ejection (Fiorotto and Rinaldo 1992; Annandale et al. 1998; Liu et al. 1998; Fiorotto and Salandin 2000; Bollaert 2004b). Pressure waves traveling through joints can be reasonably explained by transient wave theory. Nevertheless, no fully transient wave method, accounting for effects such as oscillatory or resonance waves, is actually available. The major reason is that, considering slab or block lengths of only a few meters and pressure wave celerities of $O(10^2-10^3)$ m/s, transient effects cannot be generated by macroturbulent eddies as appearing in plunge pools and stilling basins.

This paper focuses on the assessment of a realistic representation of the resistance of the rock against breakup and of the development of a fully transient wave analysis of dynamic water pressures in thin bounded media. This has been accomplished by near-prototype scaled measurements of water pressures in simulated rock joints, due to high-velocity jet impact, and by numerical modeling of the measured pressures. Application of these pressures to failure criteria of jointed rock results in a physically based model to evaluate scour. This model estimates the ultimate or equilibrium scour depth as well as the time evolution of scour formation (Bollaert 2002b, 2004a).

Experimental Modeling of Pressures in Joints

Test Facility

An experimental installation has been designed for simultaneous measurements of dynamic water pressures at plunge pool bottoms and inside underlying artificially created rock joints. The main elements of the installation are the plunging high-velocity jet, the plunge pool and the jointed rock mass (Fig. 1, Bollaert and Schleiss 2001a, 2003b).

The impacting jet has been modeled by means of a cylindrical outlet. The plunge pool has been simulated by a 3 m diameter Lucite basin. The jointed rock has been modeled by two 100 mm

[1]President, AquaVision Engineering Ltd., P.O. Box 73 EPFL, CH-1015 Lausanne, Switzerland; formerly, Senior Research Associate at Laboratory of Hydraulic Constructions, Swiss Federal Institute of Technology, CH-1015 EPFL, Switzerland. E-mail: erik.bollaert@aquavision-eng.ch

[2]Professor, Laboratory of Hydraulic Constructions (LCH), Swiss Federal Institute of Technology, CH-1015 EPFL, Switzerland. E-mail: anton.schleiss@epfl.ch

Note. Discussion open until August 1, 2005. Separate discussions must be submitted for individual papers. To extend the closing date by one month, a written request must be filed with the ASCE Managing Editor. The manuscript for this paper was submitted for review and possible publication on April 2, 2003; approved on July 9, 2004. This paper is part of the ***Journal of Hydraulic Engineering***, Vol. 131, No. 3, March 1, 2005. ©ASCE, ISSN 0733-9429/2005/3-1–XXXX/$25.00.

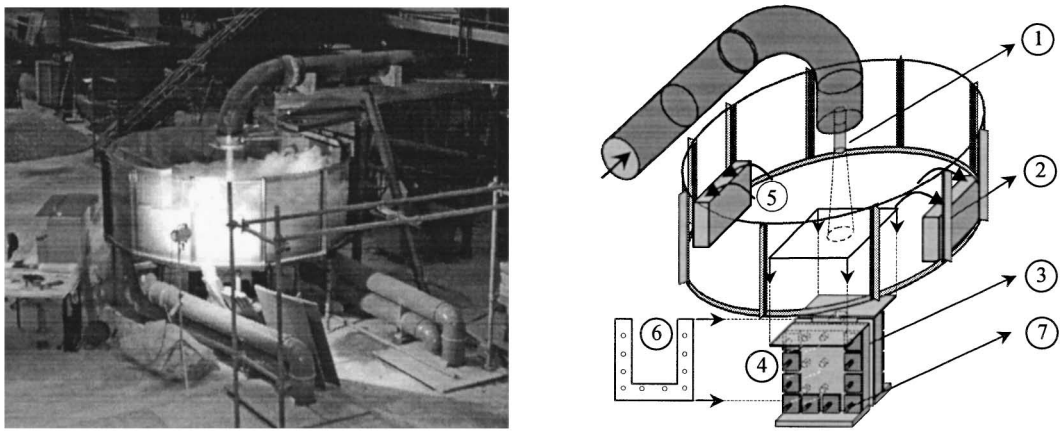

Fig. 1. Photo and perspective view of experimental facility: (1) jet, (2) cylindrical basin, (3) prestressed steel structure, (4) PC-DAQ and pressure sensors, (5) restitution, (6) thin steel sheeting, and (7) prestressed steel bars

thick steel plates with a surface of 1 m^2. Between these two plates, a 1 mm thin stainless steel strip has been sandwiched by ten prestressed steel bars (36 mm diameter, see Fig. 2). The general shape of the rock joint to simulate is then defined by cutting its boundaries out of the steel strip. This creates a cavity in the steel strip that, once the strip installed between the two 100 mm thick main plates, represents the rock joint opening. As such, by performing different cuts, any possible one- or two-dimensional rock joint of constant thickness can be simulated and inserted in between the two main plates. The geometrical precision of the steel parts is ±0.1 mm.

Kulite XTC micropressure sensors have been installed in the plunge pool bottom, in the region of jet impact, and also in between the main steel plates (Fig. 3). These sensors have a measuring surface with a diameter of 3 mm, flush-mounted along the inside of the main plates. This allows measuring pressures that travel through the simulated opening at an acquisition rate of maximum 20 kHz. An eight-channel 14 bit analog to digital data acquisition board has been used to register the pressures. The accuracy of the sensors was found at ±0.05% of their full scale (170 m of absolute pressure head), while the total error of the acquisition system has been estimated at about twice this value. Most of the test runs have been performed at an acquisition rate of 1,000 Hz, which procured sequences of 65 s. Such sequences provided a good synergy between ergodicity of statistical values and appropriate acquisition speed.

Emphasis has been given on the near-prototype character of the facility, by using mean jet velocities of up to 35 m/s and by using planar but prototype-scaled joints. The discharges were between 40 and 125 L/s. The accuracy of the discharge measurements is less than 1%. The jet diameter is 57 or 72 mm and the initial plunge pool water depths are set between 0 and 1 m. The plunge pool water depth aims at diffusing the impacting jet such that prototype aeration and turbulence conditions are generated in the turbulent shear layer at the water–rock interface. These conditions are mainly governed by the velocity and the initial turbulence intensity of the impacting jet. The former is at prototype

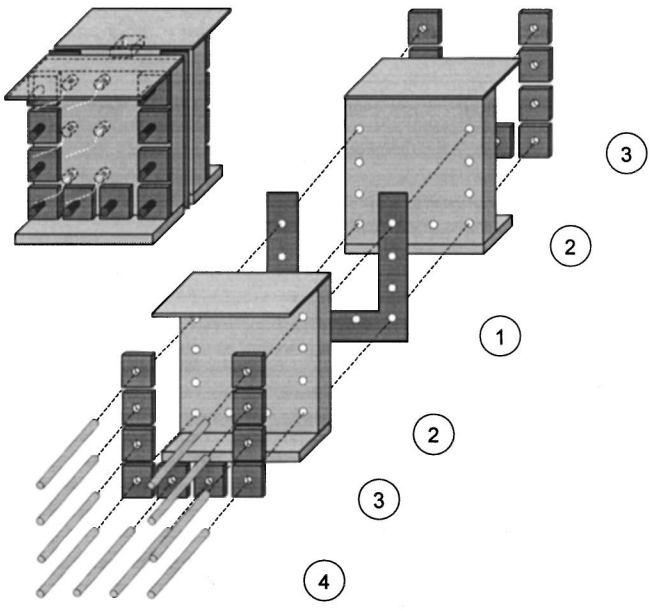

Fig. 2. Elements that simulate jointed rock: (1) stainless steel sheet, (2) galvanized steel plates, (3) support plates for steel bars, (4) set of ten prestressed steel bars. Steel sheet presented here simulates two-dimensional rock joint of 1 mm thickness.

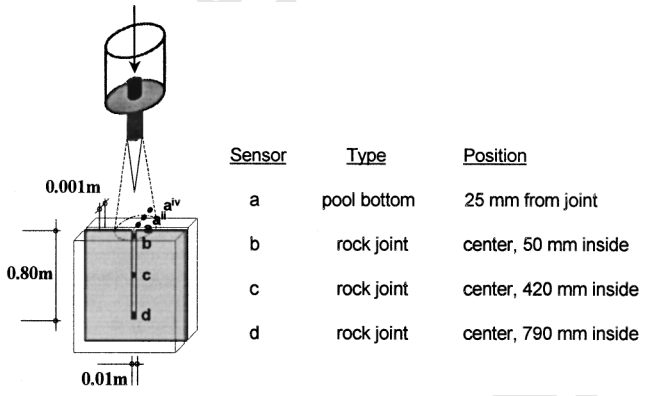

Fig. 3. Detailed view of I-shaped closed-end rock joint and of impacting jet. Pressure sensor *a* is situated at pool bottom, close to rock joint, while sensors *b*, *c*, and *d* are located at beginning, in middle, and at end of joint.

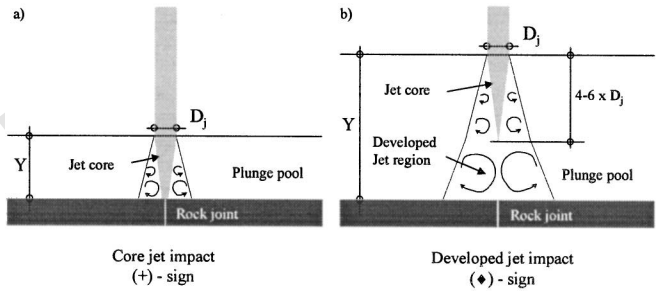

Fig. 4. Plunging jets: (a) core jet impact (+ symbol, for $Y/D_j < 4-6$); (b) developed jet impact (♦ symbol, for $Y/D_j > 4-6$)

scale. The latter has been measured and was found representative for prototype falling jets (values of 3–6%). Hence, it is believed that the facility generates frequency spectra in good agreement with spectra of real high-velocity air–water jets (Bollaert and Schleiss 2001a; Bollaert et al. 2002b).

Plunge Pool Bottom Pressures

Jet impact in a pool is governed by diffusion. Momentum exchange with the pool creates a progressively growing shear layer, characterized by an increase of the jet's total cross section and a convergence of the core jet region (Fig. 4). Dynamic pressures acting on the water–rock interface can so be generated by core jet impact, appearing for small plunge pool depths Y, or by developed jet impact (shear layer), appearing for ratios of pool depth to jet thickness Y/D_j higher than 4–6 (for plunging jets) (Ervine and Falvey 1987). The exact ratio depends on jet outlet conditions and jet aeration and stability effects. In the present study, a value between 5 and 6 was deduced from the tests.

The most relevant statistical characteristics are the mean dynamic pressure coefficient C_{pa} and the root-mean-square (RMS) of the fluctuating dynamic pressures C'_{pa}, measured at the jet's centerline. These coefficients define the pressures as a function of the incoming kinetic energy of the jet, i.e., $V^2/2g$, and expressions can be found in Ervine et al. (1997) or Bollaert et al. (2002b) (see Table 1). Fluctuating dynamic pressures are function of the air concentration at impact and of the initial turbulence intensity Tu of the jet, which depends on the type and geometry of the outlet structure (see Table 2).

Transient Rock Joint Pressures

The impact of a jet onto a rock joint exhibits all elements characteristic for a resonator system. The jet generates a cyclic excitation at the joint entrance and the joint provides the necessary resonating volume. In case of a pressure wave celerity of 1,000 m/s, the transient pressure excitation onto a joint of (maximum) 10 m long can create significant oscillatory conditions for a frequency range of excitation beyond 35–70 Hz, based on the fundamental resonance mode $f_{res}=c_j/(4L_f)$ or $f_{res}=c_j/(2L_f)$ for a closed or open-end one-dimensional resonator system. This seems hardly possible in the case of macroturbulent flow governed by large eddies and with its spectral energy mainly at low frequencies (<25 Hz; Toso and Bowers 1988).

Table 1. Polynomial Coefficients for Different Turbulence Intensities of Jets (Bollaert 2002a)

Tu (%)	a_1	a_2	a_3	a_4	Type of jet
<1	0.000220	−0.0079	0.0716	0.000	Compact
1–3	0.000215	−0.0079	0.0716	0.050	Lowly turbulent
3–5	0.000215	−0.0079	0.0716	0.100	Moderately turbulent
>5	0.000215	−0.0079	0.0716	0.150	Highly turbulent

Table 2. Estimation of Initial Jet Turbulence Intensity Tu Based on Type of Outlet Structure (Bollaert et al. 2002a, b)

Type of outlet	Tu (%)
1. Free overfall	0–3
2. Ski-jump outlet	3–5
3. Intermediate outlet	3–8
4. Bottom outlet	3–8

The present tests indicate that high-velocity jets have significant energy beyond this frequency range (Bollaert and Schleiss 2003b). Typical pressure fluctuations measured in an I-shaped one-dimensional rock joint (see Fig. 3) are presented in Fig. 5.

This figure compares pressures measured at the pool bottom, close to the rock joint entrance [sensor (a)], with simultaneously measured pressures at the end position inside the joint [sensor (d)]. Significant amplifications occur, generating peak pressures of up to several times the maximum surface pressures. The amplifications follow a cyclic pattern, governed by the fundamental resonance frequency of the joint. In between two pressure peaks, a relatively long period of very low, near-atmospheric pressures can be distinguished. The peak pressures are defined by a characteristic pressure amplitude Δp_c and a characteristic frequency f_c. They can be directly related to the pool bottom pressure fluctuations (RMS values) by means of an amplification factor Γ^+, which expresses the ratio of the maximum observed peak pressure C^+_{pd} to the C'_p coefficient of the surface pressures that generate the peaks (Fig. 6). The corresponding amplification factor between maximum and RMS pressures at the pool bottom is generally close to 3–4 (Ervine et al. 1997). Empirical curves for maximum and minimum values of the amplification factor Γ^+ can be found in Bollaert (2002a, 2004a).

The observed scatter is believed to be caused by the air content inside the joint and by low-frequency fluctuations (stability effects) of the jet (Bollaert 2002a). High peak pressures occur when no high air content is available and when significant pressure diffusion by leakage of water out of the joint is impossible. This assumption might only be valid in the case of tightly sealed rock joints. For such rock joints, the upper bound of the maximum pressure values should thus be used. For rock joints with several

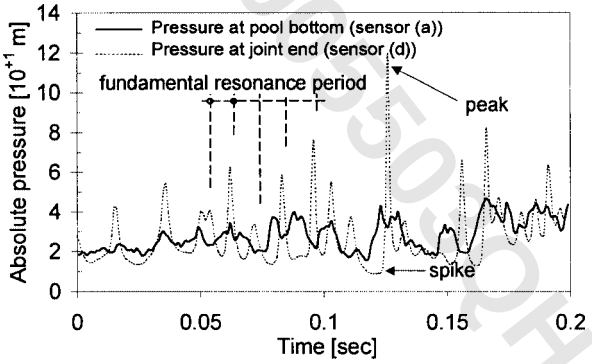

Fig. 5. Measured pressure signals in time domain for developed jet impact. Comparison is made between sensors (a) and (d).

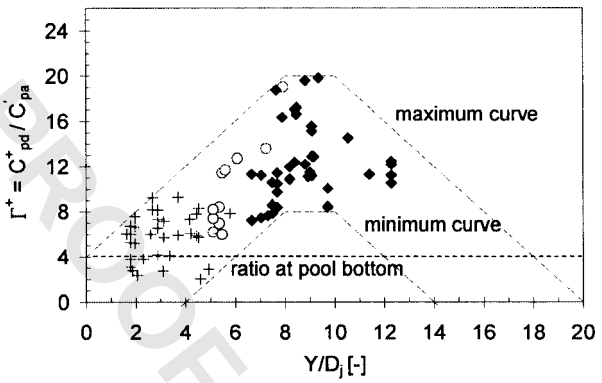

Fig. 6. Amplification factor Γ^+ between maximum pressures inside joint and root-mean-square pressures at water–rock interface, as function of Y/D_j. Measured data are circumscribed by maximum curve and minimum curve, and represent core jet impact (+) and developed jet impact (♦).

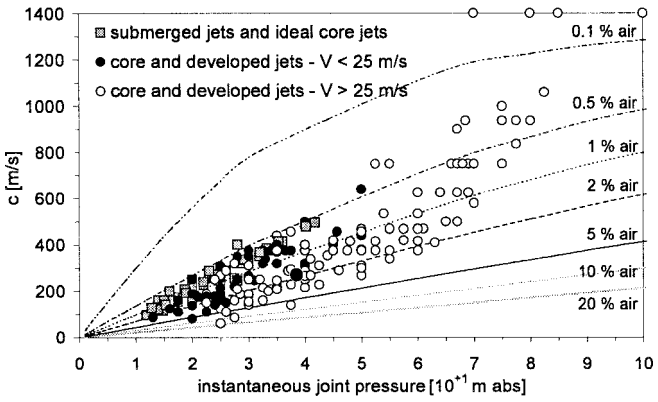

Fig. 7. Determination of instantaneous wave celerity c (m/s) as function of instantaneous pressure value $p(t)$ inside joint. Pressures are absolute and in 10^{+1} m of head. Results are for submerged and ideal core jets (obtained for convergent outlet), and for core or developed jets at low and high jet velocities, respectively.

side branches, or joints that are not tightly healed, more air could be present inside. Thus, the lower bound values are more appropriate.

Numerical Modeling of Pressures in Joints

A numerical modeling of pressures in joints has been performed in collaboration with the Laboratory of Hydrodynamics in Liège (Belgium) to verify and assess the physical phenomena that are responsible for the amplification and resonance effects observed during the experiments. These phenomena can be studied based on the curves expressing wave celerity versus pressure.

Celerity–Pressure Curves

Jet impact generates a lot of air in a plunge pool. At the interface with the rock, flow containing free air as well as air in solution penetrates into the joints and generates transient pressure waves. The celerity of the waves changes with pressure and is considered to be defined by the ideal gas law and by Henry's law (Bollaert 2002b,a; Bollaert and Schleiss 2003b).

The relationship between the time-averaged celerity c_{mean} and the time-averaged absolute pressure p_m in one-dimensional joints has been derived from the pressure measurements. The mean celerities were determined based on the fundamental resonance frequency as defined by the power spectral density of the measured pressures and by assuming a theoretical fundamental resonance frequency of $f_{\text{res}}=c_{\text{mean}}/(4L_f)$. This procures the time-averaged air concentration in the joint.

The instantaneous concentration is defined based on cross correlations between different measurement locations, taken at high acquisition rates (5–20 kHz). This is presented in Fig. 7. This figure first shows a series of celerity–pressure curves that are valid for a certain volume of free air at standard atmospheric pressure conditions (Wylie and Streeter 1978). Each curve represents a constant mass of free air in the joint. Second, measured data points are presented. The mass of free air in the joint is clearly not a constant value. The measured celerity–pressure curves are significantly steeper than the ones for a constant mass of free air. This suggests that air is being generated during pressure drops and dissolved during pressure peaks, following Henry's law. This would also suggest that air solution and dissolution occurs quasi-instantaneously, while generally a certain incubation time exists (Schweitzer and Szebehely 1950).

For practical engineering purposes, two statements can be made. First of all, wave celerities less than 100 m/s have been observed. This means that resonance frequencies in rock joints might be very low and, thus, easily generated by an impacting high-velocity jet. Second, the celerity depends on the instantaneous pressure value in the joint, which makes the transient problem highly nonlinear and difficult to assess. A numerical modeling using different celerity–pressure curves has been developed and compared with the measurements.

Model Equations and Assumptions

A numerical simulation of the measured transient water pressures in rock joints makes use of the derivative form of the one-dimensional transient flow equations for a homogeneous two-component air–water mixture (Bollaert 2002b; Bollaert et al. 2002a)

$$\frac{\partial p}{\partial t} + \frac{c^2}{g} \cdot \frac{\partial V}{\partial x} = 0 \tag{1}$$

$$\frac{\partial(\eta, V)}{\partial t} + \frac{\partial}{\partial x}(\beta V^2) + g \cdot \frac{\partial p}{\partial x} + \frac{1}{2} \cdot \frac{\lambda}{D} \cdot V \cdot |V|^e = 0 \tag{2}$$

in which p=pressure head (m); V=mean velocity (m/s); c =pressure wave celerity (m/s); and D=hydraulic diameter. The following assumptions apply to the present model:

1. For a thin joint, the hydraulic diameter D is twice the joint thickness.
2. λ, η, and β account for steady, unsteady, and nonuniform velocity distribution friction losses. λ is based on Colebrook–White and β is considered equal to 1.
3. The friction terms incorporate all other possible energy losses, such as heat or momentum exchange between the air and the water.
4. For turbulent flow conditions inside the joint, the exponent e is taken equal to 1. However, as a result of the narrow geometry, the Reynolds numbers are very low [$\sim O(10^2)$] and laminar flow revealed to procure better results. Hence, the corresponding exponent e has been taken equal to 0.

5. The two-component air–water mixture inside the joint is simulated as a pseudofluid with average properties and, thus, only one set of conservation equations.
6. The density is hardly modified by the gas and, at relatively small gas contents, may approximate the density of the liquid.
7. Any possible mass or momentum transfer between the two components is excluded.
8. No slip velocity or heat transfer between the two phases is considered.
9. The homogeneous flow model has been applied. No further assumption is made regarding the distribution of air throughout the joint.
10. Test run periods were of 10 s per optimization. This period was found to provide an appropriate balance between correct numerical analysis and acceptable computation time. For every run, the first second of calculations has been systematically omitted from the optimization process, in order to avoid influences of the initial condition. Preliminary tests with a sinusoidal input signal have shown that most of these influences die out after some tenths of seconds.

Methodology

The air concentration inside the joints is mathematically introduced by a constitutive relationship between the celerity $c(x,t)$ and the pressure $p(x,t)$. This replaces any kind of transfer (heat, mass or momentum) that might occur between the air and the water and has the advantage of simplicity. It is dependent on both space and time. Based on the shape of the measured relationships, quadratic curves are assumed, written as follows:

$$c(x,t) = k_1 + k_2 \cdot p(x,t) + k_3 \cdot p^2(x,t) \tag{3}$$

in which k_1, k_2, and k_3=parameters that allow optimization of the model. This means that five parameters apply to the present model: λ, η, k_1, k_2, and k_3.

The numerical scheme that is used to solve a weak formulation of the set of Eqs. (1)–(3) is a second-order finite-volume scheme. As the experimental pressure measurements revealed the appearance of violent transient and highly nonlinear wave phenomena, it is obvious that a shock-capturing scheme, introducing a fit amount of numerical dissipation without excessive smearing of the peak pressures, is preferable. The numerical code defines an unsteady pressure signal as weak upstream boundary condition and imposes a zero flow velocity as weak downstream boundary condition [at the end of the joint, Fig. 8(a)]. The upstream pressure signal has been taken from the experimental measurements made at the entrance of the rock joint. The boundary conditions have been presented in Fig. 8(a), together with the numerical grid. The optimization of the friction losses parameters λ, η, and of the k parameters is based on a comparison of the histograms and power spectra of the computed pressure values with the corresponding measured values [Fig. 8(c)]. The optimization process

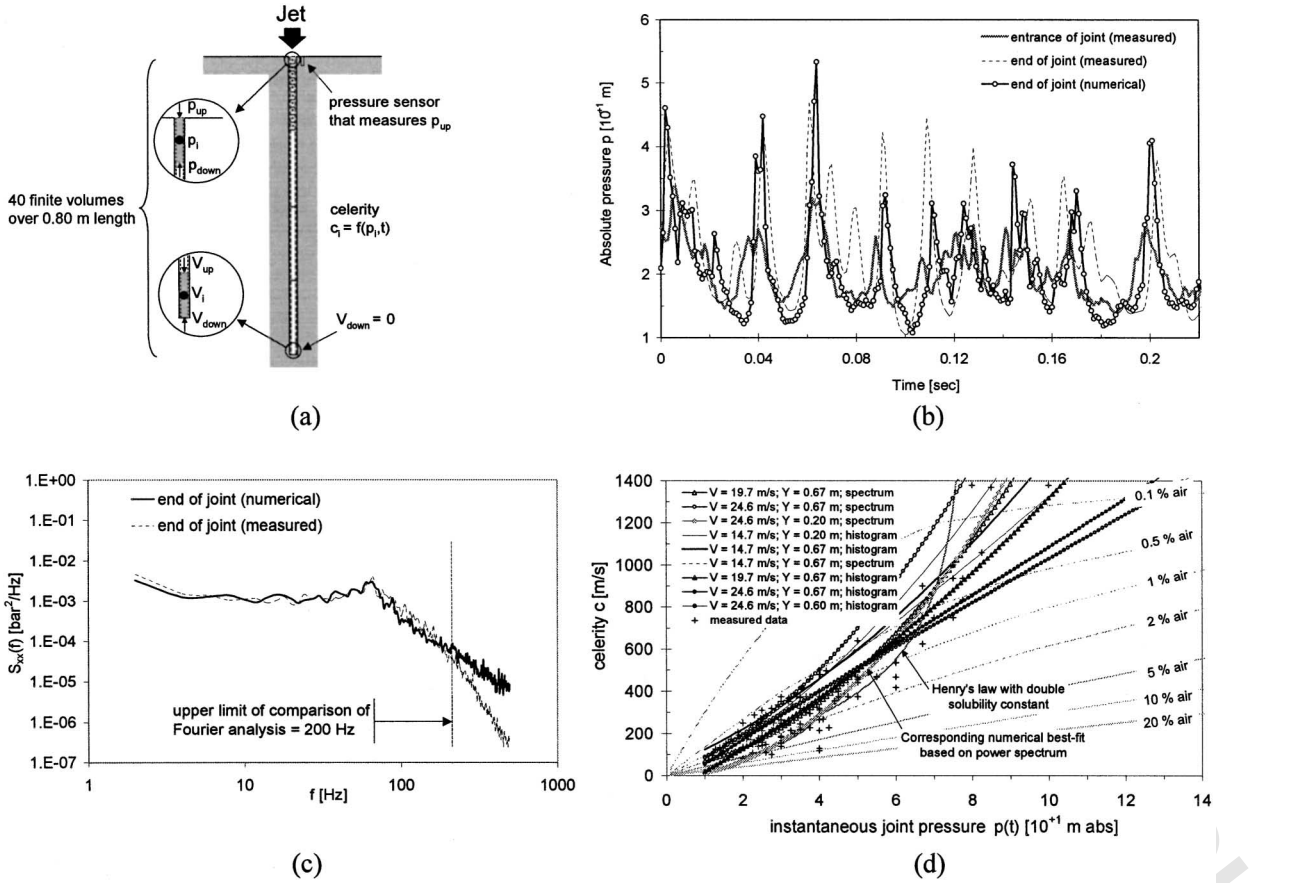

Fig. 8. (a) Definition of numerical grid and of upstream and downstream boundary conditions; (b) comparison of experimental and numerical derived pressures at end of I-joint; (c) corresponding power spectral densities; and (d) celerity–pressure relationships and comparison with measured data points for different jet velocities and plunge pool depths

has been performed by using genetic algorithms that minimize the differences between measured and computed spectra and histograms by means of a least-square criterion. A range of possible values has been initially defined for each of the parameters, and the genetic algorithm searches for the combination of parameter values that procures the best fit for the $c-p$ curve. This optimization process took about 24 h per test case on a Pentium IV processor and has been performed for pool depths ranging from 0.20 m (core jet impact) to 0.67 m (developed jet impact) and for jet outlet velocities V_j between 10 and 30 m/s.

Results

The main results of the optimization of the parameters are summarized in Table 3. A direct comparison of measured and computed pressures signals is presented in Fig. 8(b). A good agreement has been obtained for both the pressure peaks and the pressure spikes. The time intervals that were measured between two consecutive peaks is also respected in the computed pressure signal. Comparison of the spectral contents of both measured and computed pressure signals shows that the joint resonating frequencies are well reproduced and that a very good agreement exists for frequencies of up to 200 Hz. Above this value, the computed signal overestimates the energy content, probably because of the absence in the numerical model of thermal dissipation effects generated by high-frequency compression and expansion of air bubbles. An overview of numerically optimized celerity–pressure curves, valid for an I-shaped one-dimensional rock joint, is presented in Fig. 8(d).

Comprehensive Scour Model

A physically based engineering model has been developed for prediction of the ultimate scour depth of jointed rock (Bollaert 2002b, 2004a). The scour model describes two major failure criteria of a jointed rock mass. The first one, the comprehensive fracture mechanics (CFM) method, determines the ultimate scour depth by expressing instantaneous or time-dependent crack propagation. The second one, the dynamic impulsion (DI) method, describes the ejection of rock blocks from their mass due to sudden uplift pressures. This situation may occur once a certain degree of breakup of the rock mass has been attained.

The structure of the scour model distinguishes different modules: the falling jet, the plunge pool, and the rock mass. The latter implements the two aforementioned failure methods. Emphasis is given on the physical parameters that are necessary to accurately describe the different processes.

Table 3. Parametric Results of Genetic Algorithm Optimization for Test Runs of 10 s Each and for Different Jet Velocities and Plunge Pool Depths

V_j (m/s)	Y (m)	k_1	k_2	k_3	λ	η	Criterion
14.7	0.20	65	10.0	0.000	0.20	1.00	Histograph
14.7	0.67	125	9.0	0.071	0.35	1.00	Histograph
14.7	0.67	77.1	12.0	0.021	0.47	1.00	Spectrograph
19.7	0.67	22	10.2	0.047	0.53	1.14	Histograph
19.7	0.67	70	5.0	0.143	0.58	1.00	Spectrograph
24.6	0.20	−10.7	0.5	0.173	1.00	0.80	Spectrograph
24.6	0.67	55.7	11.4	0.000	0.71	1.00	Histograph
24.6	0.67	10.7	6.4	0.147	0.78	1.00	Spectrograph

Falling Jet Module

This module describes how the hydraulic and geometric characteristics of the jet are transformed from its point of issuance from the dam down to the plunge pool (Fig. 9). Three main parameters characterize the jet at issuance: the velocity V_i, the diameter (or width) D_i, and the initial jet turbulence intensity Tu.

The trajectory of the jet through the atmosphere is based on ballistics and drag forces encountered by the jet through the air and will not be further outlined herein. The basic output is the exact location of jet impact, the jet trajectory length L and the jet velocity at impact V_j. Knowledge of the jet trajectory length L allows determining the contraction of the jet due to gravitational acceleration. This conducts to the jet diameter at impact D_j. This diameter is essential to determine the Y/D_j ratio in the plunge pool.

Second, the turbulence intensity Tu defines the lateral spread of the jet δ_{out} (Ervine et al. 1997). Superposition of the outer spread to the initial jet diameter D_i results in the outer jet diameter D_{out}, which is used to determine the extent of the zone at the water–rock interface where severe pressure damage may occur. The corresponding expressions can be found in Bollaert (2004a).

Furthermore, the angle of the jet at its point of impact is neglected in the present analysis, which is reasonable for impingement angles that are close to the vertical (70–90°). For smaller impingement angles, it is proposed to use the same hydrodynamic parameters as for vertical impingement, but to redefine the water depth in the pool Y as the exact trajectory length of the jet through the water cushion, and not as the vertical difference between water level and pool bottom.

Plunge Pool Module

The second module refers to the hydraulic and geometric characteristics of the natural or constructed plunge pool downstream of the dam and defines the statistical characteristics of the hydrodynamic loading at the water–rock interface. The water depth Y in the plunge pool is an essential parameter of the scour model. For

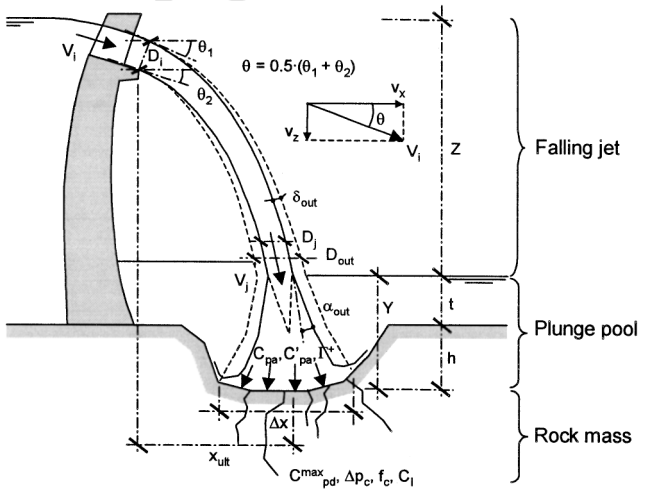

Fig. 9. Definition sketch of main parameters of free overfall jet plunging into pool and breaking up rock mass

near-vertically impacting jets, it is defined as the difference between the water level and the bedrock level at the point of impact. The water depth increases with increasing outflow discharge and with progressive scour formation. Initially the plunge pool water depth Y equals the tailwater depth t (Fig. 9). During scour formation, the water depth Y has to be increased with the depth of the already formed scour h. Possible mounding is not accounted for but can be easily integrated in the present model. Knowledge of the plunge pool water depth Y and the jet diameter at impact D_j (defined in the falling jet module) determines the ratio of water depth to jet diameter at impact Y/D_j. This ratio is directly related to diffusion characteristics of the jet.

It is assumed that the root-mean-square values of the pressure fluctuations at the water–rock interface, expressed by the C'_{pa} coefficient, depend on the Y/D_j ratio and on the initial turbulence intensity Tu. The measured data have been approximated by a polynomial regression. The regression form was obtained through curve fitting of the bandwidth of upper data as given by Ervine et al. (1997). The exact regression location is based on the present prototype-scaled test results and is presented in Fig. 10 and in Table 2 for different turbulence intensity levels. Each curve corresponds to a certain degree of (low-frequency) jet stability. The curves are valid up to a Y/D_j ratio of 18–20. For higher ratios, the C'_{pa} value that corresponds to a ratio of 18–20 should be used. Compact jets are smooth-like during their fall, without any possible source of low-frequency instability. Highly turbulent jets have a Tu value higher than 5%. In between, two other curves have been defined. They are applicable to lowly or moderately turbulent jets.

Second, the nondimensional mean dynamic pressure coefficient C_{pa} decreases with increasing air content in the plunge pool. This, however, is without consideration of the low-frequency turbulences of the jet, which have a significant impact on the mean pressure value. As such, on the test facility, the higher mean values were obtained at very high air concentrations, because the jet was more stable under such circumstances. Based on the experimental results (Bollaert 2002b), it is proposed to relate the choice of C_{pa} to the choice of C'_{pa} in the following manner: the higher the chosen curve of root-mean-square values, the lower the choice for the mean pressure value. This is logical considering that turbulent or unstable jets generate high root-mean-square values, but low mean pressures.

The mean and fluctuating pressure coefficients decrease radially outwards of the jet's centerline following exponential relationships as defined in Bollaert (2002b).

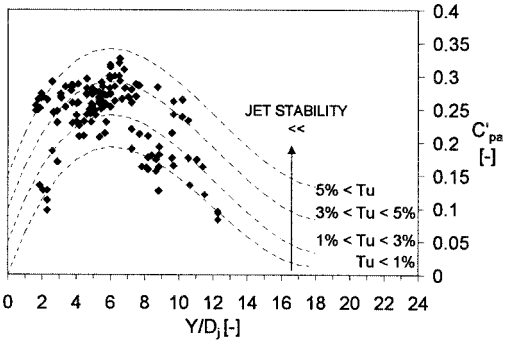

Fig. 10. Nondimensional coefficient C'_{pa} of dynamic pressure fluctuations. Data are approached by four polynomial regressions as function of jet stability (Bollaert et al. 2002a,b).

Rock Mass Module

Comprehensive Fracture Mechanics Method

The plunge pool module defines the parameters of the hydrodynamic loading at the bottom of the plunge pool. This is used as input for determination of the hydrodynamic loading inside open-end or closed-end rock joints. The governing parameters for the CFM method are as follows (Fig. 9):

1. Maximum dynamic pressure coefficient C_p^{max};
2. Characteristic amplitude of pressure cycles Δp_c; and
3. Characteristic frequency of pressure cycles f_c.

The maximum dynamic pressure coefficient C_p^{max} is obtained through multiplication of the root-mean-square pressure coefficient C'_{pa} with the amplification factor Γ^+, and by superposition with the mean dynamic pressure coefficient C_{pa}. The product of C'_{pa} times Γ^+ results in a pressure coefficient C^+_{pd}. As such, the maximum pressure value is written

$$P_{max}\ (\text{Pa}) = \gamma \cdot C_p^{max} \cdot \frac{\phi \cdot V_i^2}{2g} = \gamma \cdot (C_{Pa} + \Gamma^+ \cdot C'_{Pa}) \cdot \frac{\phi \cdot V_i^2}{2g} \quad (4)$$

where ϕ stands for the kinetic energy correction factor, generally assumed close to the unity.

The characteristic amplitude of the pressure cycles Δp_c is determined by the characteristic maximum and minimum pressures of the cycles. The minimum pressures are quite constant and always close to the standard atmospheric pressure. The maximum pressures are chosen equal to the C_p^{max} value.

The characteristic frequency of the pressure cycles f_c is determined by the joint resonator system and depends on the air concentration in the joint α_i and the length of the joint L_f. The air content inside the joints can be directly related to the air content in the plunge pool (Bollaert and Schleiss 2001b; Bollaert 2002a). For practice, a first hand estimation for f_c considers a mean celerity of 100–200 m/s (depending on the mean pressure value) and joint lengths of typically 0.5–1 m. This results in frequencies of 25–100 Hz.

The resistance of the rock against cyclic pressures is described by fatigue stresses occurring at the tip of the joint and responsible for joint propagation. This is expressed by linear elastic fracture mechanics, which assumes a perfectly linear elastic, homogeneous, and isotropic material. Despite these simplifying assumptions, application to fractured rock becomes complicated when accounting for all relevant parameters (Atkinson 1987; Whittaker et al. 1992; Andreev 1995).

Therefore, a simplified methodology is proposed here (Bollaert 2002b, 2004a), accounting for the most important physical phenomena but in a comprehensive way. It is applied in the present section to partially jointed rock. Pure tensile hydrodynamic loading of rock joints is described by the stress intensity factor K_I. This parameter represents the amplitude of the stresses in the rock material that are induced by the water pressures at the tip of the joint. The corresponding resistance of the joint against propagation is expressed by its fracture toughness value K_{Ic}.

The stresses induced in the rock are characterized by a stress intensity factor K_I as follows:

$$K_I = \eta \cdot P_{max} \cdot F \cdot \sqrt{\pi \cdot L_f} \quad (5)$$

in which K_I is in MPa$\sqrt{}$m; P_{max} is in MPa; and η is a factor that accounts for a nonhomogeneous pressure distribution along the joint and is generally close to 0.8.

The boundary correction factor F depends on the type of crack and on its persistency, i.e., its degree of cracking defined as a/B

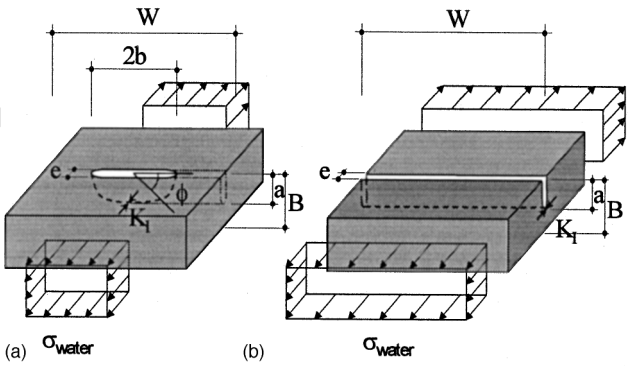

Fig. 11. Proposed framework for basic geometrical configurations of intermittently jointed rock: (a) semielliptical joint and (b) single edge joint. Water pressures are applied from outside joints.

in Fig. 11, where two basic configurations for partially jointed rock are presented. The water pressure in the joints is applied from outside. The choice of the most relevant geometry depends on the type and the degree of jointing of the rock. The first crack is of semielliptical or semicircular shape and, pertaining to the laterally applied water pressure P_{max}, partially sustained by the surrounding rock mass in the two horizontal directions. As such, it is the geometry with the highest possible support of surrounding rock. Corresponding stress intensity factors should be used in the case of low to moderately jointed rock. The second crack is single-edge notched and of two-dimensional nature. Support from the surrounding rock mass is only exerted perpendicular to the plane of the notch and, as a result, stress intensity factors will be substantially higher than for the first case. Thus, it is appropriate for significantly to highly jointed rock.

A summary of F values is presented in Fig. 12. For practice, values of 0.5 or higher are considered to correspond to completely broken-up rock, i.e., the DI method (see further) becomes more applicable than the CFM method. For values of 0.1 or less, it is considered that a pure tensile strength approach is more plausible than a fracture mechanics approach. However, most of the values in practice can be considered between 0.20 and 0.40, depending on the type and number of joint sets, the degree of weathering, joint interdistances, etc. A first-hand broad-brush calibration of this parameter has been performed in Bollaert et al. (2002) by comparison with Annandale's erodibility index method.

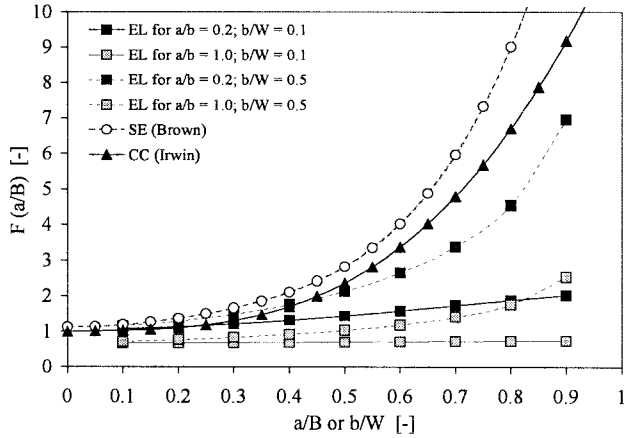

Fig. 12. Comparison of different boundary correction factors F for computation of stress intensity at tip of rock joint

The fracture toughness K_{Ic} strictly depends on a vast range of parameters. The most important are the tensile strength T or the unconfined compressive strength (UCS). Also, corrections are made to account for the loading rate and the in situ stresses. The so corrected fracture toughness is defined as the in situ fracture toughness $K_{I,ins}$ and is based on a regression of available literature data

$$K_{I\ ins,T} = (0.105 \text{ to } 0.132) \cdot T + (0.054 \cdot \sigma_c) + 0.53 \quad (6)$$

$$K_{I\ ins,UCS} = (0.008 \text{ to } 0.010) \cdot UCS + (0.054 \cdot \sigma_c) + 0.42 \quad (7)$$

in which σ_c represents the confinement horizontal in situ stress and T, UCS, and σ_c are expressed in MPa.

Crack propagation distinguishes between brittle (or instantaneous) crack propagation and time-dependent crack propagation. Brittle crack propagation will occur if

$$K_I \geq K_{I,ins} \quad (8)$$

If this is not the case, crack propagation needs a certain time to happen. This is expressed by a classical fatigue equation

$$\frac{dL_f}{dN} = C_r \cdot (\Delta K_I / K_{Ic})^{m_r} \quad (9)$$

in which L_f=joint length and N=number of pressure cycles. C_r and m_r are rock material parameters that can be determined by fatigue tests and ΔK_I=difference of maximum and minimum stress intensity factors at the joint tip. To implement time-dependent crack propagation into a comprehensive engineering model, the parameters m_r and C_r have to be known. They are qualitatively known for static fatigue as a function of the type of rock (see Table 4), but have to be determined by appropriate calibration of the model.

Dynamic Impulsion Method

The fourth hydrodynamic parameter is the maximum dynamic impulsion C_I^{max} in an open-end rock joint (underneath a rock block). This parameter is obtained by a time integration of the net forces on the rock block

Table 4. Fatigue Exponent m_r and Fatigue Coefficient C_r for Different Rock Types (Bollaert 2002a, based on Atkinson 1987)

Type of rock	Exponent m_r	Coefficient C_r
Arkansas novaculite	0.5	1.0E−8
Mojave quartzite	10.2–12.9	3.0E−10
Tennessee sandstone	4.8	4.0E−7
Solenhofen limestone	8.8–9.5	1.1E−8
Falerans micrite	8.8	1.1E−8
Tennessee marble	3.1	2.0E−6
Westerley granite	11.8–11.9	8.0E−10
Yugawara andesite	8.8	1.1E−8
Black gabbro	9.9–12.2	4.0E−9–5.0E−10
Ralston basalt	8.2	1.8E−8
Whin Sill dolerite	9.9	4.0E−9

$$I_{\Delta tpulse} = \int_0^{\Delta tpulse} (F_u - F_o - G_b - F_{sh}) \cdot dt = m \cdot V_{\Delta rpulse} \quad (10)$$

in which F_u and F_o=forces under and over the block; G_b =immerged weight of the block; and F_{sh} represents the shear and interlocking forces. The shape of a block and the type of rock define the immerged weight of the block. The shear and interlocking forces depend on the joint pattern and the in situ stresses. As a first approach, they can be neglected by assuming that progressive dislodgment and opening of the joints occurred during the breakup phase of the rock mass. The pressure field over the block is governed by the turbulent shear layer of the jet. The pressure field under the block corresponds to transient pressure waves inside open-end rock joints.

The pressures or forces are considered independent of any block movement, which seems plausible for a high peak pressure during a small time interval.

The first step is to define the instantaneous differences in forces over and under the block. For periods Δt during which net uplift forces exist, the time integral has been taken. This results in net impulsions I and a maximum net impulsion I^{max}.

Second, I^{max} is made nondimensional by defining the impulsion as the product of a net force and a time period. For this, the net force is transformed into a pressure. This pressure can then be made dimensionless by dividing it by the incoming kinetic energy $\phi \cdot V^2/2g$. This results in a net uplift pressure coefficient C_{up}. The time period is made dimensionless by the travel period characteristic for pressure waves inside rock joints, i.e., $T=2L_f/c$, in which L_f stands for the total joint length and c for the mean wave celerity. This results in a time coefficient T_{up}.

Hence, the dimensionless impulsion coefficient C_I is defined by the product $C_{up} \cdot T_{up} = V^2 \cdot L/g \cdot c$ (m s). These parameters are presented in Fig. 13. The maximum net impulsion I^{max} is finally obtained by multiplication of the value for C_I by $V^2 \cdot L/gc$.

For jet velocities V_j higher than 20 m/s, a quite constant value for C_I of 0.35 has been observed during the experiments. As a function of the Y/D_j ratio, the observable scatter is quite low. For core jets, a value of 0.6 to 0.8 seems plausible. For developed jets, the values are situated between 0.2 and 0.5.

For practice, it is proposed to use the following polynomial expression

$$C_I = 0.0035 \cdot \left(\frac{Y}{D_j}\right)^2 - 0.119 \cdot \left(\frac{Y}{D_j}\right) + 1.22 \quad (11)$$

Failure of a rock block is expressed by the displacement it undergoes due to the net impulsion [Eq. (10)]. This kinetic energy is then transformed into a net uplift displacement h_{up}. The displacement that is necessary to eject a rock block from its matrix is difficult to define. Factors such as the degree of interlocking of the blocks can be of great significance and are hard to determine. A very tightly jointed rock mass will need a displacement that is equal to or higher than the height of the block. Less tightly jointed rock will probably be uplifted more easily. The necessary displacement is thus a model parameter that needs to be calibrated for appropriate application of the model.

Case Study of Cabora-Bassa Dam

The Cabora-Bassa Dam, a double curvature arch dam (Fig. 14), is located on the Zambezi River in Mozambique and has a total spillway discharge capacity of 13,100 m^3/s (at a maximum reservoir level of 326 m a.s.l.). The corresponding tailwater level is at 225 m a.s.l. with a depth of nearly 50 m above the natural

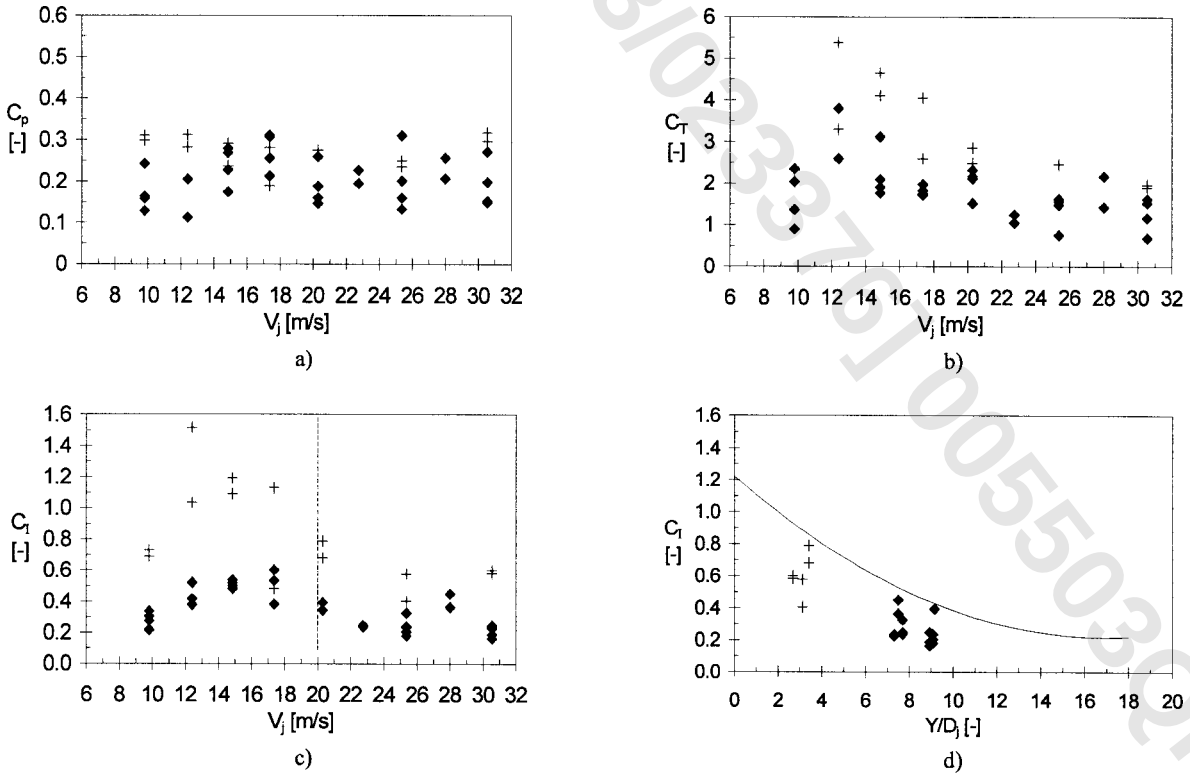

Fig. 13. Nondimensional impulsion coefficients for pressures inside open-end rock joints: (a) C_p as function of V_j; (b) C_T as function of V_j; (c) C_I as function of V_j; and (d) C_T as function of Y/D_j

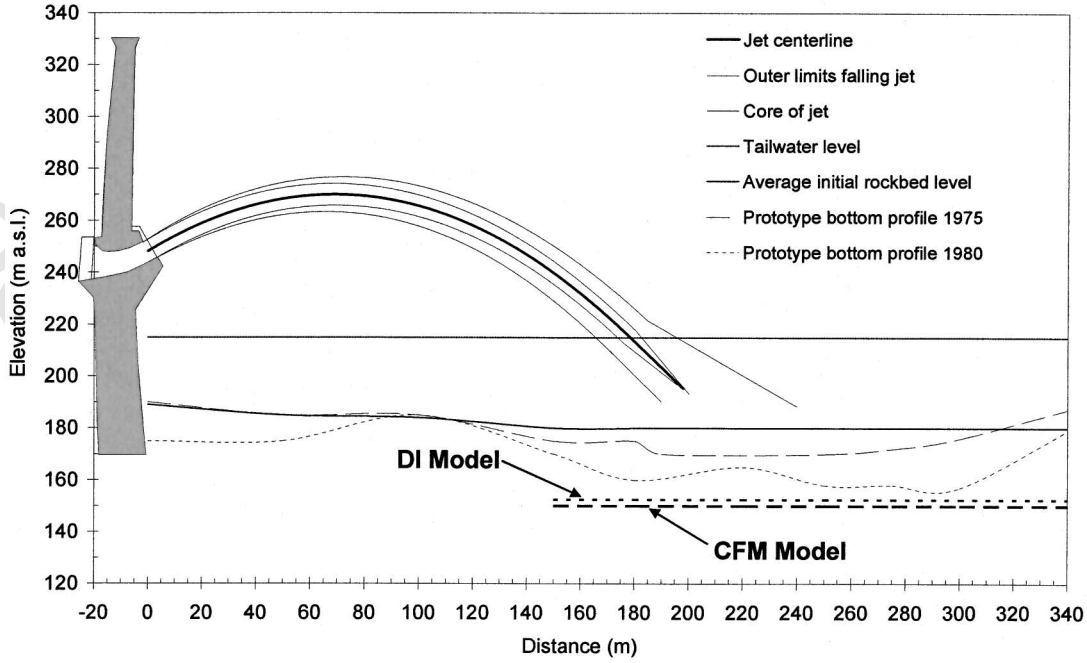

Fig. 14. Cabora-Bassa Dam: Prototype measured and computed scan profiles

riverbed. The spillway consists of eight identical sluice gates with a height of 6 m and a width of 7.8 m. The exit lip of the gates is at elevation 244.30 m a.s.l. and makes an angle of 32.3° with the horizontal. The riverbed is very irregular and has its elevations varying from 170 to 180 a.s.l. The rock is mainly granitoide gneiss with little cracking, but with a few gabbro and lamprophire dykes.

Hydraulic model tests at a 1/75 scale have been conducted at LNEC, Lisbon, Portugal (Ramos 1982). A moveable bed model was used, made with gravel weakly aggregated with aluminous cement. The test results predicted the maximum scour depth at an elevation of 150 m a.s.l. and a downstream distance from the jet outlet of 250 m.

The prototype behavior of the dam is characterized by two important operating periods. The first one happened in 1975 during 42 days, for a discharge of 6,000 m^3/s (=4 gates). The scour depth after this operation was measured at about 170 m a.s.l.. The tailwater level was at 215 m a.s.l.

The second period occurred in 1978. The spillway was being operated for four and a half consecutive months as presented in Table 5 (Ramos 1982). The maximum reservoir level was at 327.74 m a.s.l. An extensive survey of the scour pit in 1980 showed that the deepest point of the scour pit was situated at 158 m a.s.l., i.e., 22 m deeper than the original riverbed. This occurred at a downstream distance from the jet outlet ranging from 240 to 260 m.

Table 5. Spillway Operating Conditions in 1978 at Cabora-Bassa Dam (Ramos 1982)

No gates	Discharge (m^3/s)	Period	Duration (days)
>4	6,300	3 June–23 July	139
>5	8,200	13 March–18 April	36
>6	9,800	17 March–12 April	26
>7	11,500	22 March–5 April	14
>8	13,100	23 March–5 April	13

Jet and Plunge Pool Characteristics

The diameter of the jet at issuance from the dam has been estimated as the equivalent hydraulic diameter of the 6 m × 7.8 m rectangular outlet. This results in an initial jet diameter D_i =7.7 m. The jet trajectory has been calculated based on ballistic equations and air drag. The initial turbulence intensity of the jet has been estimated at Tu=5% (Table 1). This resulted in a jet impact velocity V_j of 41.6 m/s and an impact diameter D_j of 7.2 m. The outer jet diameter was estimated at D_{out}=17 m. The jet breakup length L_b has been estimated at 152 m of trajectory length, corresponding to a downstream distance from the jet outlet x_{ult} of around 145 m. The jet is considered just broken-up at impact in the plunge pool.

The air concentration at jet impact is considered very high (~60%) and the available excitation capacity of the jet is most probably decreased by the jet breakup. Therefore, it is not plausible to account for high amplification effects of the pool bottom pressures inside the rock joints and, thus, Γ^+ values close to the minimum curves (Fig. 6) have been applied. The corresponding C_p^{max} values have been calculated based on Eq. (4) and were found between 2.5 and 3 for Y/D_j values of up to 10 but rapidly decreased at higher Y/D_j ratios.

Rock Mass Characteristics and Calibration of Methods

According to Fig. 11, the model assumes semicircular joints (a/b=1.0 and b/W=0.5) with a persistency a/B of 0.2 for a total possible length of 1 m. The circular shape and low persistency have been chosen based on the statement of little cracking of the rock mass (Ramos 1982) and based on the agreement between the CFM method and Annandale's erodibility index (EI) method (Bollaert 2002b). The boundary correction factor F is equal to 0.7, according to Fig. 12.

A UCS value of 13 MPa has been used. This value was defined by application of Annandale's EI method to the observed

Table 6. Ultimate Scour Depth Based on Comprehensive Fracture Mechanics Method

Type of jet	Y (m)	ϕV_j (m/s)	D_j (m)	Y/D_j	C_{stat}	C_{pa}	C'_{pa}	C_{max}	K_I (MPa m$^{0.5}$)	KI_{xy} (MPa m$^{0.5}$)	Crack propagation	Elevation (m a.s.l.)	Total time (days)
Developed	47.5	41.6	7.24	6.6	0.40	0.36	0.24	2.7	1.13	1.47	Fatigue	179.9	0
Developed	50.1	41.6	7.24	6.9	0.42	0.32	0.24	2.9	1.19	1.47	Fatigue	178.0	16
Developed	52.7	41.6	7.24	7.3	0.44	0.29	0.24	3.0	1.25	1.48	Fatigue	176.0	26
Developed	55.3	41.6	7.24	7.6	0.46	0.26	0.23	3.1	1.30	1.48	Fatigue	174.1	33
Developed	58.3	41.6	7.24	8.1	0.49	0.24	0.23	3.2	1.35	1.48	Fatigue	171.9	39
Developed	60.9	41.6	7.24	8.4	0.51	0.22	0.22	3.2	1.32	1.49	Fatigue	170.0	43
Developed	63.5	41.6	7.24	8.8	0.53	0.20	0.22	3.1	1.30	1.49	Fatigue	168.1	49
Developed	66.5	41.6	7.24	9.2	0.56	0.18	0.21	3.0	1.27	1.50	Fatigue	165.9	58
Developed	69.1	41.6	7.24	9.5	0.58	0.17	0.20	3.0	1.24	1.50	Fatigue	164.0	68
Developed	71.7	41.6	7.24	9.9	0.60	0.16	0.19	2.9	1.21	1.51	Fatigue	162.1	81
Developed	74.3	41.6	7.24	10.3	0.62	0.15	0.19	2.7	1.13	1.51	Fatigue	160.1	102
Developed	77.2	41.6	7.24	10.7	0.65	0.13	0.18	2.5	1.04	1.51	Fatigue	158.0	157
Developed	82.4	41.6	7.24	11.4	0.69	0.12	0.16	2.1	0.88	1.52	Fatigue	154.1	538
Developed	88.0	41.6	7.24	12.2	0.74	0.10	0.14	1.8	0.74	1.53	Fatigue	150.0	2,911
Developed	94.7	41.6	7.24	13.1	0.79	0.09	0.12	1.4	0.60	1.54	Fatigue	145.1	24,236

prototype scour depth. By assuming plausible values for the other rock mass characteristics (degree of jointing, block size, joint roughness) and based on a comparison between computed and observed scour depths, a plausible UCS value was derived. Based on Annandale (1995), this value corresponds to hard rock. The horizontal in situ stress field is considered to reflect an overburden pressure of 100 m, with a horizontal to vertical stress ratio of $K_0=1$. The narrow shape of the surrounding valley justifies this value. The m_r parameter [Eq. (9)] is chosen equal to 10, based on the assumption that granitoide gneiss is more sensible to fatigue than pure granite (with a value of 12). The C_r parameter has been calibrated based on the prototype observations and was found equal to 1.0E-7.

For the DI method, the ratio of height to side length of the rock blocks is chosen equal to 1, following the cubic block assumption made by Ramos (1982). Eventual shear forces between the blocks are neglected. Appropriate calibration of the ratio of uplift displacement to block height h_{up}/z resulted in a critical value of around 0.20. For ratios equal to or higher than 0.20, the blocks are considered ejected from the surrounding mass.

Ultimate Scour Depth by Comprehensive Fracture Mechanics and Dynamic Impulsion Methods

The results are presented in Tables 6 and 7. After calibration of the C_r and h_{up}/z parameters, the CFM method indicates results that are in good agreement with the prototype observations: a depth of 170 m a.s.l. is attained after 43 days of discharge (42 on prototype), and the depth of 158 m a.s.l., observed on the site after the 1978 spillage of 139 days is obtained by the CFM method after 114 days of additional spillage. Once calibrated, the method is able to predict further scouring as a function of discharge duration. Hence, further scouring down to 154 m a.s.l. would need another 380 days of discharge. After, the phenomenon slows down, due to jet diffusion effects, and an additional scouring down to 150 m a.s.l. would need about 2,500 days of discharge. Stating that the 1978 discharges were exceptional, and accounting for a reasonable lifetime of the dam, it can be argued that the elevation of 150 m a.s.l. constitutes a practical limit of ultimate scour depth, in accordance with the model tests.

The DI method makes use of a maximum net impulsion C_I

Table 7. Ultimate Scour Depth Based on Dynamic Impulsion Method

Type of jet	Y (m)	fV_j (m/s)	D_j (m)	Y/D_j	CI	I_{max} (N s)	I_{net} (N s)	V_{up} (m/s)	h_{up} (m)	h_{up}/z (—)	Uplift	Elevation (m a.s.l.)
Developed	62.379	42	7.24	8.6	0.46	7,876	5,874	3.46	0.61	0.61	Uplift	168.9
Developed	63.492	42	7.24	8.8	0.45	7,724	5,723	3.37	0.58	0.58	Uplift	168.1
Developed	65.347	42	7.24	9.0	0.43	7,479	5,477	3.22	0.53	0.53	Uplift	166.7
Developed	66.46	42	7.24	9.2	0.42	7,335	5,333	3.14	0.50	0.50	Uplift	165.9
Developed	69.057	42	7.24	9.5	0.41	7,009	5,008	2.95	0.44	0.44	Vibrations	164.0
Developed	71.653	42	7.24	9.9	0.38	6,656	4,655	2.74	0.38	0.38	Vibrations	162.1
Developed	74.25	42	7.24	10.3	0.37	6,363	4,361	2.57	0.34	0.34	Vibrations	160.1
Developed	77.218	42	7.24	10.7	0.35	6,046	4,044	2.38	0.29	0.29	Vibrations	158.0
Developed	79.814	42	7.24	11.0	0.33	5,784	3,783	2.23	0.25	0.25	Vibrations	156.0
Developed	82.411	42	7.24	11.4	0.32	5,537	3,536	2.08	0.22	0.22	Vibrations	154.1
Developed	84.637	42	7.24	11.7	0.31	5,337	3,336	1.96	0.20	0.20	Stability	152.5
Developed	87.975	42	7.24	12.2	0.29	5,029	3,028	1.78	0.16	0.16	Stability	150.0
Developed	90.572	42	7.24	12.5	0.28	4,831	2,830	1.66	0.14	0.14	Stability	148.1

$=C_{up}\cdot T_{up}$ as defined in Fig. 13. Due to the high aeration rate, the wave celerity is defined at 100 m/s. The theoretically necessary displacement of one times the height of the block is already attained at an elevation of 176 m a.s.l. The scour depth of 158 m a.s.l., observed on the prototype after the 1978 discharge period, corresponds to a h_{up}/z ratio of 0.30. The ultimate scour depth based on the dynamic uplift criterion, however, should be somewhat deeper, and has been chosen at 152 m a.s.l., corresponding to a h_{up}/z ratio of 0.20. This calibration reasonably agrees with the ultimate depths found by the CFM method and observed during the model tests.

Conclusions

A physically based model to evaluate the ultimate scour depth in jointed rock, formed by high-velocity jet impact, is presented. This model is based on near-prototype experimental investigations of the dynamic pressure fluctuations at plunge pool bottoms and inside artificially created, underlying rock joints. Also, a one-dimensional two-phase numerical modeling of the measured transient pressures has been performed. The numerically computed pressures were in good agreement with the measured ones. Pressures in closed-end joints were found of highly cyclic character and have been assessed by their characteristic amplitude and frequency. Pressures in open-end joints (underneath rock blocks) have been directly related to the corresponding pool bottom pressures, resulting in a net uplift impulsion on rock blocks.

The scour model represents a comprehensive assessment of hydrodynamic fracturing of closed-end rock joints (CFM method) and of dynamic uplift of so formed single rock blocks (DI method). Emphasis is given on the physical parameters that are necessary to accurately describe the phenomenon. These parameters are defined such that a practicing engineer can still handle them. This guarantees the comprehensive character of the model, without neglecting basic physics behind it.

The scour model has been applied to the well-known case of Cabora-Bassa in Mozambique. Simulation of the prototype-observed scour depth evolution with time has been used to calibrate the time-dependent fatigue parameters and the uplift parameters of the scour model. This also allowed prediction of future scour hole development and estimation of the ultimate scour depth.

It is obvious that the present case study has to be analyzed rather qualitatively and that further calibration of the model is appropriate. However, it clearly shows that comparison with prototype observations allows assessing existing scour formation and future scour hole development as a function of time. This confirms the promising nature of the scour model, especially for cases where past scour development has been observed and described, or where a reasonable comparison can be made with available scour behavior of similar cases. It is believed that the model will be particularly useful to predict future scour development as a function of time.

This physically based attempt to predict scour as a function of time distinguishes the present model from previously developed evaluation methods, such as Annandale's erodibility index method, and is hoped to provide the basis for development of more enhanced scour evaluation methods in the future.

Acknowledgments

The writers would like to thank Prof. M. Pirotton and S. Erpicum from the University of Liège, Belgium, for their support during the numerical modeling. The present research project has been partially funded by the Commission for Innovation and Technology (CTI), Bern, Switzerland, with financial support from the Swiss Committee on Dams and Stucky Consulting Engineers Ltd.

Notation

The following symbols are used in this paper:

b = half width of joint at surface;
b_j = jet thickness at impact (rectangular jets);
C_p = $(p_{mean}-Y)/(\phi V_j^2/2g)$;
C_p' = $(\sigma)/(\phi V_j^2/2g)$;
C_p^{max} = $(p_{max})/(\phi V_j^2/2g)$;
C_r = fatigue sensibility coefficient for rock;
c = pressure wave celerity;
D_i = jet diameter at issuance from the dam;
D_j = jet diameter at impact in plunge pool;
d = rock block size (equivalent cube size);
d_m,d_{90} = grain sizes;
e_j = joint width;
F = Froude number;
F = boundary correction factor for stress intensity;
F_o = forces over a rock block;
F_{sh} = shear forces on a rock block during uplift;
F_u = forces underneath a rock block;
f = frequency;
f_{res} = resonance frequency;
G_b = immerged weight of a rock block;
g = gravitational acceleration;
H = difference between upstream and downstream water level;
H_j = incoming total pressure head $(=\phi\cdot V_j^2/2g)$;
h = tailwater depth in riverbed downstream of scour hole;
J_a = rock joint alteration number for erodibility index method;
J_n = rock joint set number for erodibility index method;
J_r = rock joint tightness number for erodibility index method;
J_s = rock joint spacing number for erodibility index method;
j = number of joint set;
K_b = block size number for erodibility index method;
K_d = discontinuity bond shear strength number for erodibility index method;
K_h = erodibility index number;
K_{Ic} = fracture toughness of jointed rock mass;
$K_{I,ins}$ = in situ fracture toughness of jointed rock mass;
$k_{1\text{-}3}$ = coefficients of polynomial celerity–pressure relationship;
L = trajectory length of jet falling through air;
L_b = jet breakup length;
L_c = jet core length;
L_f = length of joint;
M_s = rock mass strength number for erodibility index method;
m = mass;
m_r = exponent of sensibility of rock mass to fatigue;
N = number of joint sets;
p = dynamic pressure head;

p_m = mean dynamic pressure head;
$p_{\max}$ = maximum instantaneous dynamic head;
$p_{\min}$ = minimum instantaneous dynamic head;
Q_a = air discharge;
Q_w = water discharge;
q = unitary discharge;
R = Reynolds number;
r = radial coordinate;
$S_{h,j}$ = $(f \cdot L_j)/c$, rock joint Strouhal number;
$S_{h,p}$ = $(f \cdot Y)/V_i$, plunge pool Strouhal number;
S_j = spacing of joints;
S_{xx} = power spectral density of pressure fluctuations;
T = uniaxial tensile strength of rock material;
Tu = initial jet turbulence intensity;
t = time;
UCS = unconfined compressive strength of rock material;
V_i = mean jet velocity at issuance from dam;
V_j = mean jet velocity at impact in plunge pool;
x = distance from dam to river downstream;
x_{ult} = longitudinal distance from dam of ultimate scour depth;
Y = $t+h$, total plunge pool water depth;
y = lateral direction;
Z = vertical fall length of jet through air;
z = vertical direction;
α_p = air content at point of jet impact in plunge pool;
α_r = air content in rock joint;
β = volumetric air-to-water ratio;
Γ^+ = pressure amplification factor in rock joints;
γ_s = particle or rock specific weight;
θ = jet angle with horizontal at impact in plunge pool;
λ = hydraulic friction factor (Darcy–Weisbach);
ρ_a = density of air;
ρ_r = density of rock;
ρ_w = density of water;
σ = standard deviation of pressure fluctuations (root mean square);
ϕ = coefficient of nonuniform velocity profile; and
φ = residual friction angle of joint set or plunge pool side wall.

References

Annandale, G. W. (1995). "Erodibility." *J. Hydraul. Res.*, 33(4), 471–494.

Annandale, G. W., Wittler, R. J., Ruff, J., and Lewis, T. M. (1998). "Prototype validation of erodibility index for scour in fractured rock media." *Proc., 1998 Int. Water Resources Engineering Conf.*, Memphis, Tenn.

Andreev, G. E. (1995). *Brittle failure of rock materials*, Balkema, Rotterdam, The Netherlands.

Atkinson, B. K. (1987). *Fracture mechanics of rock*, Academic, London.

Bollaert, E. (2002a). "The influence of plunge pool air entrainment on the presence of free air in rock joints." *Proc., Int. Workshop on Rock Scour*, EPFL, Lausanne, Switzerland, 137–149.

Bollaert, E. (2002b). "Transient water pressures in joints and formation of scour due to high-velocity jet impact." *Communication 13*, Laboratory of Hydraulic Constructions, EPFL, Lausanne, Switzerland.

Bollaert, E. (2004a). "A comprehensive model to evaluate scour formation in plunge pools." *Int. J. Hydropow. Dams*, 2004(1), 94–101.

Bollaert, E. (2004b). "A new procedure to evaluate dynamic uplift of concrete linings or rock blocks in plunge pools." *Proc., Int. Conf. on Hydraulics of Dams and River Structures*, Yazdandoost and Attari, eds., Teheran, Iran, 125–133.

Bollaert, E., Erpicum, S., Pirotton, M., and Schleiss, A. (2002a). "Genetic algorithm optimization of transient two-phase water pressures inside closed-end rock joints." *Proc., Int. Workshop on Rock Scour*, EPFL, Lausanne, Switzerland.

Bollaert, E., Falvey, H. T., and Schleiss, A. (2002b). "Turbulent jet impingement in plunge pools: The particular characteristics of a near-prototype physical model study." *Proc., Riverflow 2002*, Louvain-la-Neuve, Belgium, 395–403.

Bollaert, E., and Schleiss, A. (2001a). "Discussion of 'Simulation of scour process in plunging pool of loose bed-material' by Jia et al." *J. Hydraul. Eng.*, 128(7), 721–723.

Bollaert, E., and Schleiss, A. (2001b). "Air bubble effects on transient water pressures in rock fissures due to high velocity jet impact." *Proc., 29th IAHR Congress*, Beijing.

Bollaert, E., and Schleiss, A. (2003a). "Scour of rock due to the impact of plunging high velocity jets. Part I: A state-of-the-art review." *J. Hydraul. Res.*, 41(5), 451–464.

Bollaert, E., and Schleiss, A. (2003b). "Scour of rock due to the impact of plunging high velocity jets. Part II: Experimental results of dynamic pressures at pool bottoms and in one- and two-dimensional closed-end rock joints." *J. Hydraul. Res.*, 41(5), 465–480.

Ervine, D. A., and Falvey, H. R. (1987). "Behavior of turbulent jets in the atmosphere and in plunge pools." *Proc., Inst. Civ. Eng.*, 83, 295–314.

Ervine, D. A., Falvey, H. R., and Withers, W. (1997). "Pressure fluctuations on plunge pool floors." *J. Hydraul. Res.*, 35(2), 257–279.

Fiorotto, V., and Rinaldo, A. (1992). "Fluctuating uplift and lining design in spillway stilling basins." *J. Hydraul. Eng.*, 118(4), 578–596.

Fiorotto, V., and Salandin, P. (2000). "Design of anchored slabs in spillway stilling basins." *J. Hydraul. Eng.*, 126(7), 502–512.

Johnson, G. (1977). "Use of a weakly cohesive material for scale model scour tests in flood spillway design." *Proc., 17th Congress of the I.A.H.R.*, Vol. 4, Baden-Baden.

Liu, P. Q., Dong, J. R., and Yu, C. (1998). "Experimental investigation of fluctuating uplift on rock blocks at the bottom of the scour pool downstream of Three-Gorges spillway." *J. Hydraul. Res.*, 36(1), 55–68.

Quintela, A. C., and Da Cruz, A. A. (1982). "Cabora-Bassa dam spillway, conception, hydraulic model studies and prototype behaviour." *Proc., Transactions of the Int. Symp. on the Layout of Dams in Narrow Gorges*, ICOLD, Brazil.

Ramos, C. M. (1982). "Energy dissipation on free jet spillways. Bases for its study in hydraulic models." *Proc., Transactions of the Int. Symp. on the Layout of Dams in Narrow Gorges*, Vol. 1, ICOLD, Rio de Janeiro, Brazil, 263–268.

Schleiss, A. (2002). "Scour evaluation in space and time—The challenge of dam designers." *Proc., Int. Workshop on Rock Scour*, EPFL, Lausanne, Switzerland, 3–22.

Schweitzer, P. H., and Szebehely, V. G. (1950). "Gas evolution in liquids and cavitation." *J. Appl. Phys.*, 21, 1218–1224.

Toso, J., and Bowers, E. C. (1988). "Extreme pressures in hydraulic-jump stilling basin." *J. Hydraul. Eng.*, 114(8), 829–843.

Whittaker, B. N., Singh, R. N., and Sun, G. (1992). *Rock fracture mechanics*, Elsevier, Dordrecht, The Netherlands.

Wylie, E. B., and Streeter, V. L. (1978). *Fluid transients*, McGraw–Hill, New York.